The Influence of Leading-Edge Load Alleviation on Supersonic Wing Design

Christine M. Darden*
NASA Langley Research Center, Hampton, Virginia

For a planform characterized by a highly swept leading edge on the inboard region, linear theory was used to design camber surfaces which produce minimum drag due to lift at the design C_L of 0.08 and a design Mach number of 2.4. To delay the formation of leading-edge vortices, one wing was constrained to have the normal Mach number less than one everywhere along the leading edge, and the second wing was constrained to have a differential pressure coefficient of zero on the leading edge. Force tests were run on the two constrained wings, a flat reference wing, and an optimized wing with no leading-edge constraints. Results indicate that vortex strength and separation regions were mildest for a wing designed to have $\Delta C_p = 0$ at the leading edge.

Nomenclature

b	= wing span
C_D	= drag coefficient
C_L	= lift coefficient
C_M	= pitching moment coefficient
C_{M_0}	= pitching moment at zero lift
C_p	= pressure coefficient
ΔC_p	$= C_{p_{\text{lower}}} - C_{p_{\text{upper}}}$
L/D	= lift-to-drag ratio
M	= Mach number
M_N	= component of Mach normal to the leading edge
y	= axial coordinate in the spanwise direction
z	= vertical coordinate
α	= angle of attack
β	$= \sqrt{M^2 - 1}$

Subscripts

LE	= leading edge
min	= minimum value
max	= maximum value

Introduction

FOR many years, methods based on linearized theory have been used to design wings employing camber and twist for supersonic transports. Use of these linearized theory methods has shown that the most successful wing designs have been achieved when the design C_L was roughly one-half of the desired cruise C_L.[1] Milder camber surfaces result using this approach—surfaces on which the flow is modeled more accurately by the linearized methods.

A second concept which has evolved from years of study in supersonic wing design is the use of highly swept wings to reduce wave drag. At moderate angles of attack, however, highly swept wings with sharp leading edges will develop separated flow which results in a classical leading-edge vortex.[2] The explanation for this occurrence is based on the fact that flow over the wing is governed predominately by that component of the flow that is normal to the leading edge. The angle of attack with respect to the normal component of flow is a function of both the sweep angle and freestream angle of attack. Thus, for a highly swept wing at small angles of attack, the angle of incidence of the normal flow component may be increased by a factor of 2 or 3. The expansion caused by flow around such angles generates large adverse pressure gradients which promote boundary-layer separation, especially on wings with sharp leading edges. This separation generates a vortex that originates at the leading edge. The velocity and pressure distributions on the upper surface are affected by the formation of these vortices and performance is often less than expected.

Studies indicate that future requirements for military aircraft may include the need for efficient supersonic cruise and maneuver capability. These requirements necessitate designs for much higher C_L values than those designed for transport applications. In the absence of design methods that include nonlinear viscous effects, two approaches have evolved in the design of highly swept wings for high lift and low drag due to lift at supersonic speeds. One approach involves using "attainable leading-edge thrust"[3] as a guide for designing planform and leading-edge shapes that would delay separation and have thrust-producing flow. A second method employs the use available linear theory methods to design wings with twist and camber which give a minimum drag coefficient at a given lift subject to constraints placed on the design to delay flow separation. This paper discusses a design and test program conducted to assess the second method.

A planform characterized by a highly swept inboard leading edge was used in the development of camber surface designs for two wings. Within the linear theory optimization process employed, a different leading-edge pressure constraint was used for each of the two designs. The leading-edge constraints, the resultant camber, and the experimental performance of these designs are discussed.

Description of Test Program and Models

The design method used is that of Refs. 4-6 in which drag due to lift is minimized at a given total lift. Within the optimization process, constraints may be placed on pressure, z, pressure gradient, and pitching moment. Since it is the extreme pressure gradients which cause the early formation of vortices, the approach used in this study was to place limits on the loadings of the leading edge to assess its effect on the formation of the leading-edge vortices, as well as overall performation.

Presented as Paper 84-0138 at the AIAA 22nd Aerospace Sciences Meeting, Reno, Nev., Jan. 9-12, 1984; received May 21, 1984; revision received Aug. 31, 1984. This paper is declared a work of the U.S. Government and therefore is in the public domain.

*Aerospace Engineer, High-Speed Aerodynamics Division. Member AIAA.

Two wings were designed using different constraints on the leading-edge loadings. For comparison purposes, two additional models were included in the test series: one model was designed for the same conditions with no leading-edge loading constraints and an uncambered, i.e., flat, reference model was included. All four wings had identical planforms and 3% thick parabolic arc airfoils with sharp leading edges. The three cambered wings were designed to have a C_L of 0.08 at zero angle of attack at the design Mach number of 2.4. Recall that this design C_L is approximately one-half of the desired cruise C_L. All four models were tested over a range of Mach numbers from 1.8 to 2.8 with angles of attack ranging from -5 to $+8$ deg. Vapor-screen and oil-flow photographs were taken at the design Mach number for several lift conditions.

The planform selected for the series of wings is shown in Fig. 1. Note that the leading-edge sweep angles vary with spanwise position to give velocity components normal to the leading edge which vary from low subsonic for much of the inboard region to nearly sonic at the tip for the design Mach number of 2.4. A minimum body was included to house the strain gage balance for the force tests.

The first leading-edge constraint model was contrained to have $\Delta C_p = 0$ at the leading edge. This rather severe constraint requires that the leading edge be everywhere aligned with the oncoming flow at the design condition. The second model was constrained to have $M_N < 1$ everywhere along the leading edge. Leading-edge pressures for the second model were developed using elementary sweep theory with the root C_p constrained to zero, as shown in Fig. 2.

The theoretical drag-due-to-lift factors, as calculated by the design program for each of the four wings, are shown in Fig. 3. Also included is a sketch of a typical pressure distribution for each wing. Note the large leading-edge pressures for flat and unconstrained wings. As expected, the flat wing produces the highest drag-due-to-lift factor and the unconstrained model produces the lowest. The moderately constrained wing ($M_N < 1$) has the next lowest predicted drag-due-to-lift value and the severely constrained wing ($\Delta C_{p_{LE}} = 0$) has a drag-due-to-lift factor nearly as high as the flat wing.

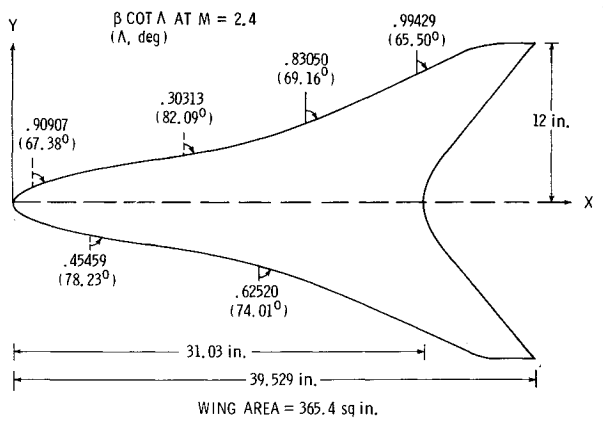

Fig. 1 Description of wing planform.

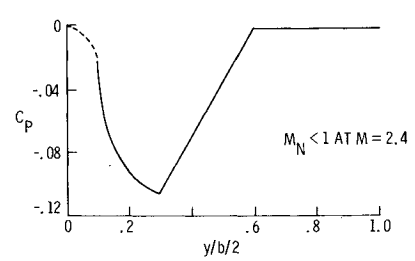

Fig. 2 Leading-edge pressure constraints using elementary sweep theory.

Test Results—Comparison with Theory

Experimental performance data at the design Mach number of 2.4 for each of the four models are shown in Figs. 4-9. Also shown on these figures are theoretical predictions from the analysis portion of the design program,[6] a nonlinear prediction[7] and a prediction using nonlinear theory which includes increments from available leading-edge thrust and vortex lift.[7] Values of skin friction drag and zero lift wave drag computed by the method of Ref. 6 have been added to drag-due-to-lift values from each of the three theoretical predictions.

For the uncambered wing, the experimental data shows better performance than the linear theory prediction shown by the solid line. Through most of the lift range shown, predictions by the nonlinear theory including thrust and

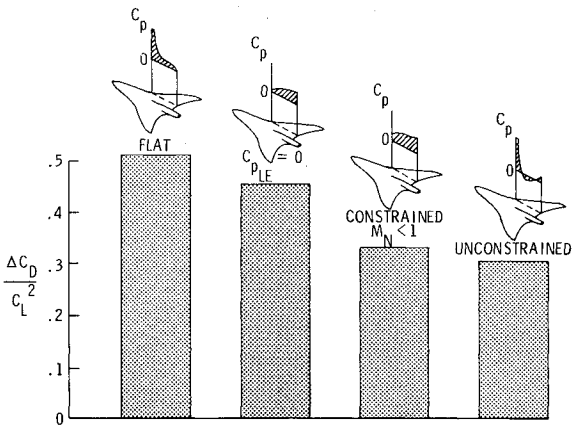

Fig. 3 Theoretical drag-due-to-lift factors.

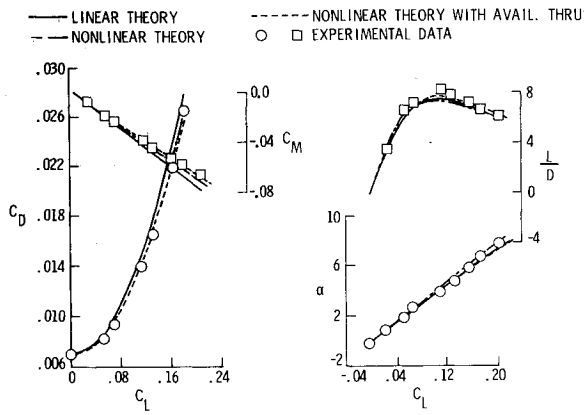

Fig. 4 Comparisons of experimental data with theoretical predictions, uncambered wing, $M = 2.4$.

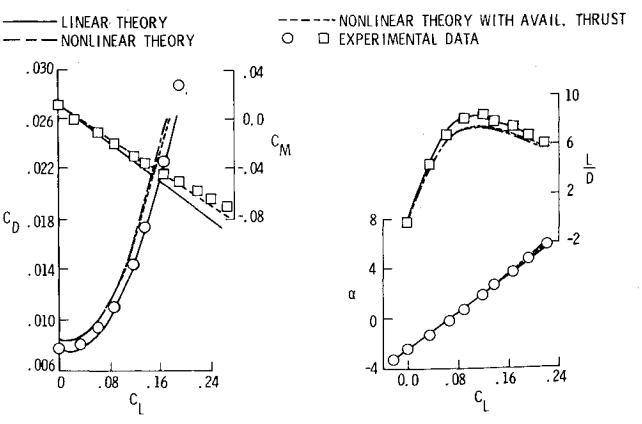

Fig. 5 Comparisons of experimental data with theoretical predictions, uncambered wing, $M = 2.4$.

vortex increments show good agreement with the experimental data for both drag levels and pitching moment. The nonlinear drag polar aligns with the linear prediction for most of the range shown, indicating that benefits in the drag profile are coming from thrust and vortex lift. The shift in the pitching moment curve comes from significant nonlinear effects and an added increment results from thrust and vortex effects.

The theoretical predictions for performance indicate a slightly lower L/D_{max} predicted by the nonlinear theory than that for linear theory. Addition of thrust and vortex increments increases L/D_{max} to a slightly higher level than predicted by linear theory. At the midrange of the lift values shown, the experimental data show higher values than any of the predicted levels. Nonlinear theory also tends to predict a lower lift for a given α as compared with linear theory as shown in the C_L vs α plot. The addition of thrust and vortex increments to the nonlinear theory increases the predicted lift coefficient to practically the same levels as those predicted by linear theory.

Experimental and theoretical performance data for the unconstrained model are shown in Fig. 5. Drag levels predicted by the linearized theory method are low at the smaller values of C_L, but agree well with the experimental data beyond C_L values of 0.1. There is practically no difference in predictions from nonlinear theory and nonlinear theory with thrust and vortex increments, and both overpredict the drag levels for this cambered wing.

The linear theory prediction for pitching moment deviates significantly from the experimental data. These data do agree rather well with the nonlinear and nonlinear with thrust curves up to a lift coefficient of about 0.2. Beyond this value of C_L, some change in flow characteristics seems to cause a destabilizing effect.

Only slight differences occur in the theoretical predictions for C_L vs α up to about $C_L = 0.16$, where the three curves tend to separate. The experimental points, while indicating a slight scatter, tend to agree most closely with the linear prediction. The best theoretical performance is predicted by linear theory as shown in the L/D vs C_L plot. The experimental points again tend to follow linear theory predictions up to $C_L = 0.14$ and then drop off to values predicted by the nonlinear theory with thrust and vortex increments at $C_L = 0.22$.

The experimental data and performance predictions for the moderately constrained model are shown in Fig. 6. A comparison of the drag polars predicted by two nonlinear methods indicates that some benefit from thrust or vortex lift is predicted beyond $C_L = 0.1$. The experimental drag values are again underpredicted by linear theory and overpredicted by the nonlinear theories. The pitching moment data are well predicted by the nonlinear theories up to about $C_L = 0.18$, at which point the experimental points break away from the theoretical prediction. If there are indeed vortex lift effects in the data, then the vortex may lift off of the wing surface at this value of C_L causing a change in pitching moment.

All of the theoretical predictions for C_L vs α are within 5% of each other except for C_L values beyond 0.16 where the nonlinear values break away from the other two predictions. It is difficult to say whether the experimental points agree with any one prediction better than the other, however, at the higher C_L values, nonlinear theory appears to most accurately predict the experimental results.

In the performance plot for the constrained ($M_N < 1$) wing, the linear theory predicts the best performance, and nonlinear theory predicts the poorest performance. The performance predicted by nonlinear theory which includes thrust falls between the other two theoretical predictions. The experimental points agree well with the nonlinear theories up to $C_L = 0.08$, at which point L/D values exceed the levels predicted by the nonlinear methods. After reaching an L/D of 8.2, experimental points drop off more rapidly than any of the theoretical methods.

Results for the most severely constrained model are shown in Fig. 7. As with the other cambered models, the nonlinear theories predict higher drag values than the linear theory at a given value of C_L. The experimental points show improved

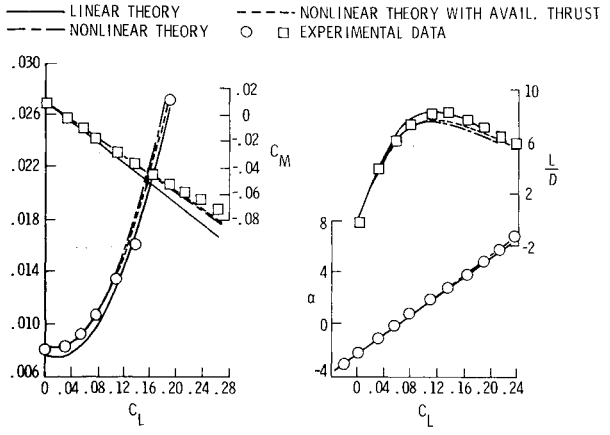

Fig. 6 Comparisons of experimental data with theoretical predictions, constrained wing, $M_N < 1$, $M = 2.4$.

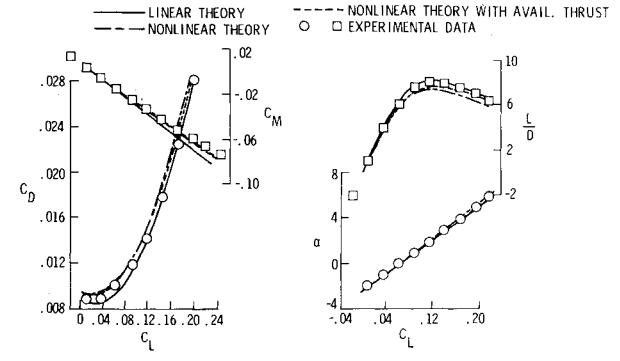

Fig. 7 Comparisons of experimental data with theoretical predictions, constrained wing, $C_{pLE} = 0$, $M = 2.4$.

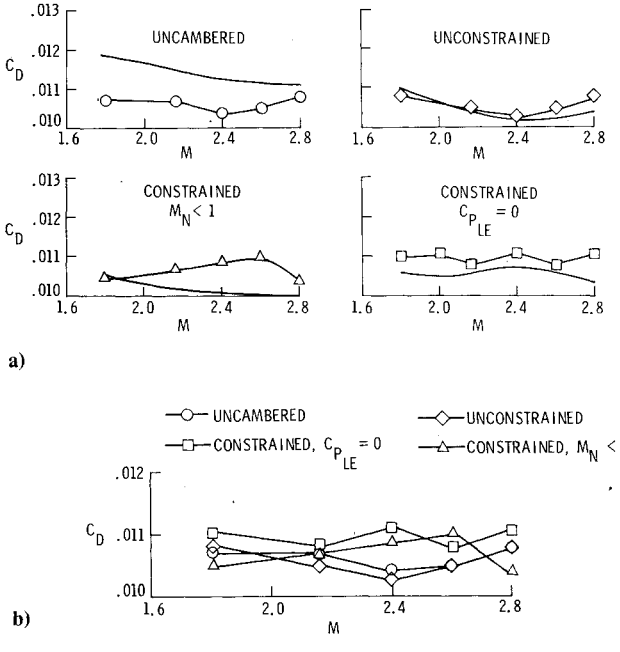

Fig. 8 Drag at design C_L of 0.08. a) Comparison of theory and experiment. b) Comparison of drag levels.

drag levels as compared to those predicted by nonlinear theory. The experimental pitching moment values are again well predicted by the nonlinear theories out to C_L values of approximately 0.18, where again the data break away from theory. The C_L vs α data agree well with the nonlinear theory with thrust effects. Experimental L/D values again generally fall between the predictions from linear and nonlinear theory except at the highest C_L value where experiment agrees well with the nonlinear theory with thrust and vortex lift.

The drag coefficient vs Mach number at the design C_L of 0.08 is shown in Fig. 8. For clarity, an expanded scale has been used for the drag coefficient. In addition to the experimental data, linear theory predictions are also shown on this figure. For the uncambered wing, the experimental drag levels are lower than those predicted. This is probably due to the effects of leading-edge thrust which is not included in the linear theory. Drag predictions for the unconstrained model agree well with the experimental points except at the highest Mach numbers. The drag of the severely constrained model ($\Delta C_{p_{LE}} = 0$) is underpredicted. Agreement between theory and experiment is least accurate for the moderately constrained ($M_N < 1$) model.

A comparison of the experimental drag at the design lift coefficients is given in Fig. 8b. The drag coefficients of the flat and unconstrained models are nearly equal at the design Mach number, while the drag of the two constrained models is about 5% higher.

Minimum drag as a function of Mach number is shown in Fig. 9. As expected, the lowest minimum drag is achieved by the flat wing and the highest by the most severely constrained wing, $\Delta C_{p_{LE}} = 0$. The theoretical predictions shown for comparison are based on linear theory and are in good agreement with the experimental values.

A comparison of the experimental drag polars for the four models at the design Mach number is shown in Fig. 10. The same trend in minimum drag of the four models is seen here. At the higher lift coefficients, however, the beneficial effects of wing camber in reducing drag can be observed. At $C_L = 0.18$, the uncambered wing gives the highest drag, with the moderately constrained, unconstrained, and severely constrained wing designs each producing an improvement in drag level.

A comparison of experimental pitching moment coefficient and angle of attack as a function of lift coefficient is given in Fig. 11. Only slight variations occur in the lift curve slope for the three cambered models. Similarly, the slopes of the pitching moment curves are all essentially the same, although there are variations in the magnitude of C_{M_0}.

Figure 12 shows the experimental performance curve for each of the wing designs as a function of lift coefficient at the design Mach number. As predicted, the peak of the L/D curve for each design occurs well beyond the model design C_L in all cases, although it is different in level and location. The overall best performance is given by the unconstrained cambered model which achieved an L/D of approximately 8.3 at $C_L = 0.11$. However, when compared with the others, each wing design shows a different range of best performance. The flat model shows best performance up to the design lift coefficient of 0.08. Between a lift coefficient of 0.08 and approximately 0.145, the unconstrained design gives the best performance. The moderately constrained model shows best performance from $C_L = 0.145$ to 0.165. Beyond 0.165, the severely constrained design gives the best performance. This better performance is attained, however, with penalties in performance at the lower lift coefficients. These results indicate that the constrained wing designs do give the best performance at the desired cruise C_L of approximately 0.16.

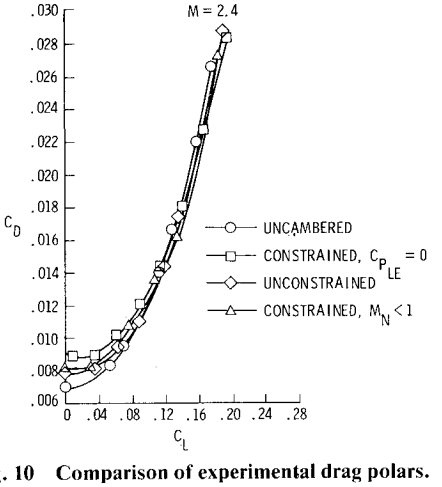

Fig. 10 Comparison of experimental drag polars.

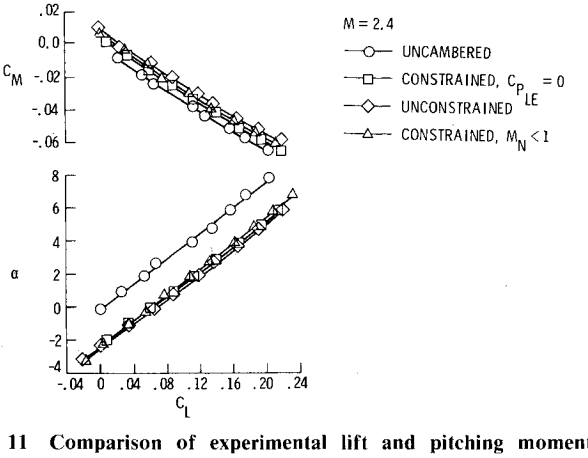

Fig. 11 Comparison of experimental lift and pitching moment results.

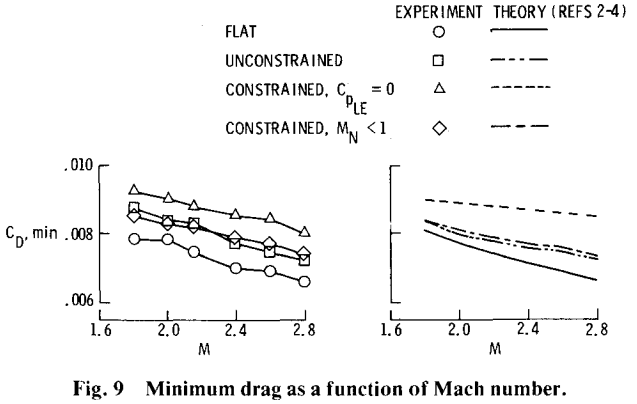

Fig. 9 Minimum drag as a function of Mach number.

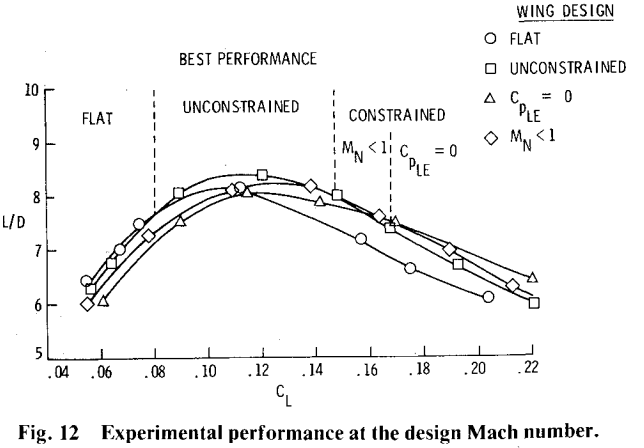

Fig. 12 Experimental performance at the design Mach number.

Flow Visualization Results

Some insight into flow patterns that occur on each of the four wing designs can be seen in the flow visualization photographs presented in Figs. 13-16. Photographs of oil flows at $\alpha = 0$ and 5 deg and a vapor-screen photograph at $\alpha = 5$ deg are shown for each model. The lift coefficient corresponding to a 5 deg angle of attack is somewhat lower than the desired cruise lift of 0.16 for the flat wing, and somewhat higher than the desired cruise lift for the optimized wings.

The top portion of Fig. 13 indicates the very smooth, attached potential flow for the uncambered wing at $\alpha = 0$ deg. At $\alpha = 5$ deg, which represents a C_L of 0.135, the photograph shows evidence of vortices trailing back over the wing from the region near the nose on the leading edge. Some slight separation is also indicated near the outboard regions of the trailing edge. The vapor screen shows evidence of the vortex from the nose region and a region of separation near the leading edge.[8]

Photographs for the unconstrained wing are shown in Fig. 14. In the photograph of the oil flow at $\alpha = 0$ deg, evidence can be seen of vortex flow behind that portion of the leading edge with greatest sweep. The vapor screen at this condition (not shown), does indicate some slight degree of separation behind the nose region. The lift coefficient of the uncontrained model at 5 deg angle of attack is approximately 0.198. The oil flow at this angle of attack shows a very complicated flow pattern. There is evidence of vortex flow just outboard of the root chord as well as several regions along the leading edge and at the tip of the trailing edge which show indications of separated flow. Also, there is strong spanwise flow all along the trailing edge. The accompanying vapor-screen photograph indicates a well-formed vortex inboard, and a separation region near the leading edge.

The flow at $\alpha = 0$ deg for the moderately constrained model (Fig. 15) appears to be smooth and attached. Although the flow has a slight spanwise tendency near the root of the trailing edge, there appears to be no separation or vortex flow. At $\alpha = 5$ deg, $C_L = 0.192$, the flow again becomes quite complicated. There is evidence of two vortices trailing behind the leading edge and extreme spanwise flow near the trailing edge. Regions of separation are seen in at least two places along the leading edge and at the trailing edge. Evidence of the vortex flow can be seen in the accompanying vapor-screen photograph which also indicates some separation near the leading edge.

Flow-visualization photographs for the most severely constrained model are shown in Fig. 16. At the design C_L,

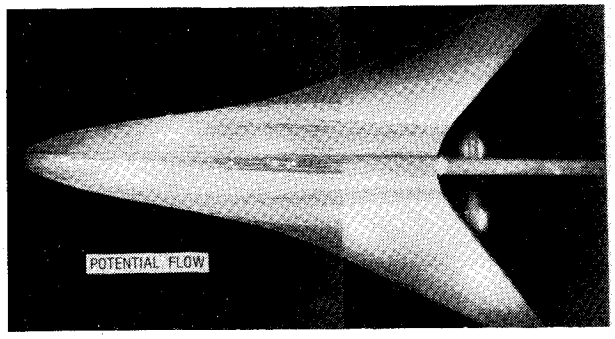

a) Oil flow at $\alpha = 0$ deg.

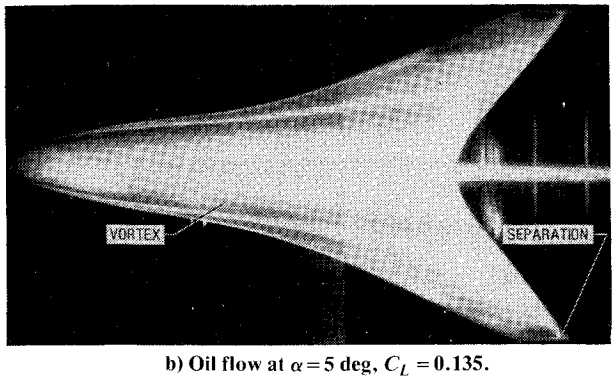

b) Oil flow at $\alpha = 5$ deg, $C_L = 0.135$.

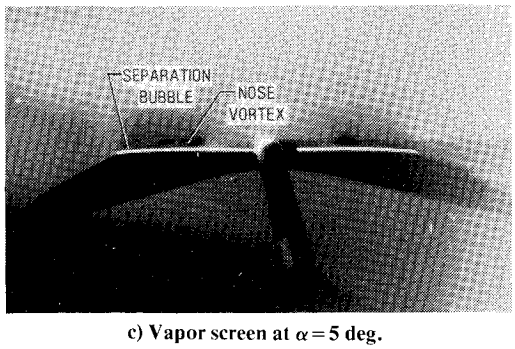

c) Vapor screen at $\alpha = 5$ deg.

Fig. 13 Flow-visualization photographs of uncambered wing, $M = 2.4$.

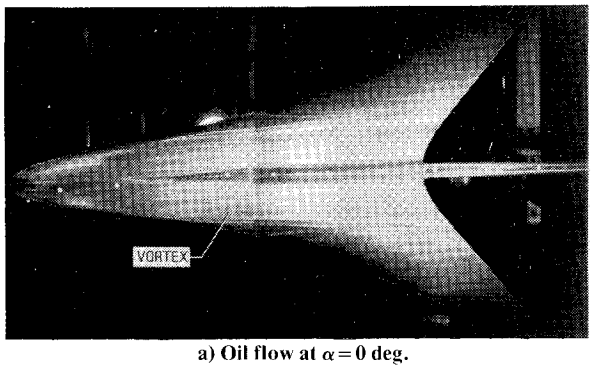

a) Oil flow at $\alpha = 0$ deg.

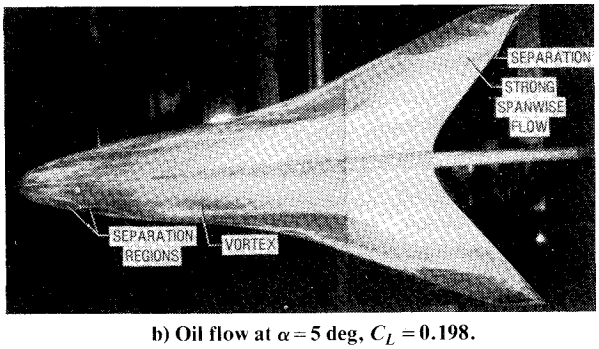

b) Oil flow at $\alpha = 5$ deg, $C_L = 0.198$.

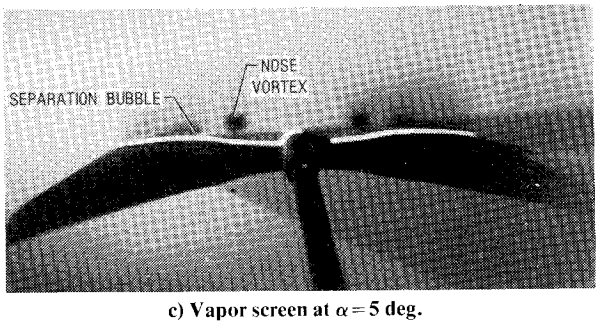

c) Vapor screen at $\alpha = 5$ deg.

Fig. 14 Flow-visualization photographs of unconstrained wing, $M = 2.4$.

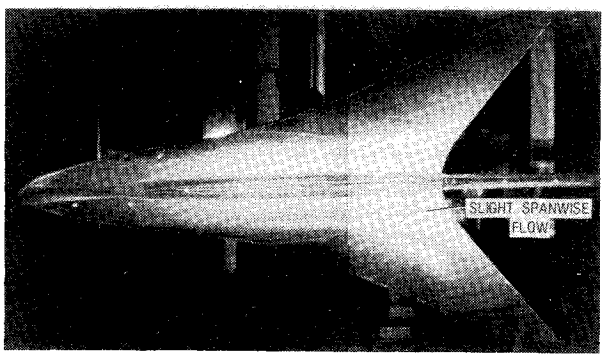

a) Oil flow at $\alpha = 0$ deg.

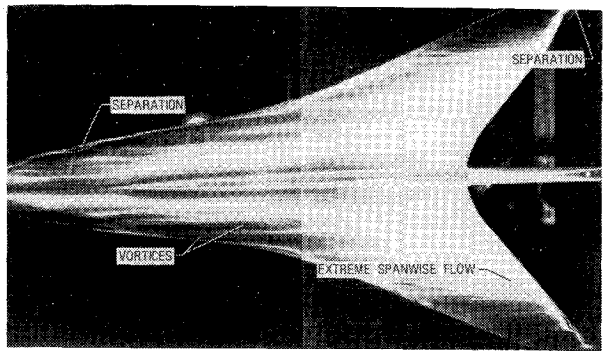

b) Oil flow at $\alpha = 5$ deg, $C_L = 0.192$.

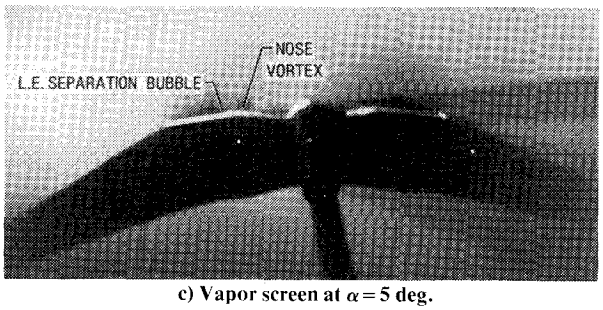

c) Vapor screen at $\alpha = 5$ deg.

Fig. 15 Flow-visualization photographs of constrained wing, $M_N < 1$, $M = 2.4$.

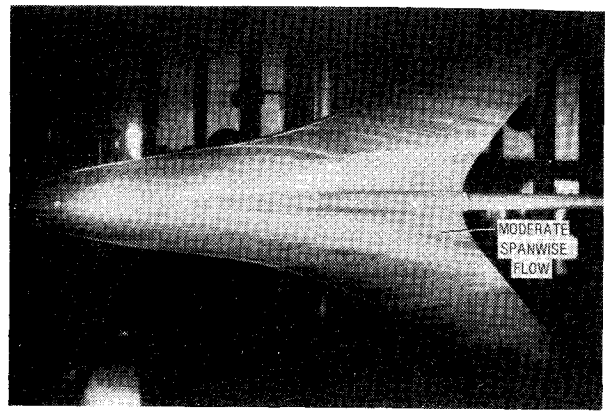

a) Oil flow at $\alpha = 0$ deg.

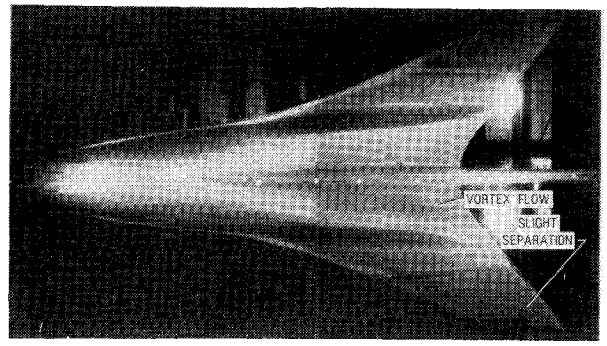

b) Oil flow at $\alpha = 5$ deg, $C_L = 0.198$.

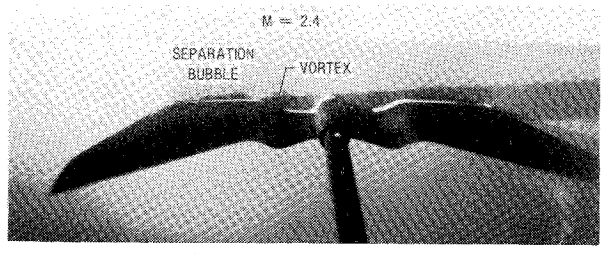

c) Vapor screen at $\alpha = 5$ deg.

Fig. 16 Flow-visualization photographs of constrained wing, $C_{pLE} = 0$, $M = 2.4$.

$\alpha = 0$, the flow near the front and outboard portions of the wing appears very smooth and attached. Although there is some spanwise flow near the root of the trailing edge which meets a slightly inward flow near the shoulder region of the wing, there is no evidence of any vortices or separation. When the wing is placed at $\alpha = 5$ deg, its accompanying lift coefficient is 0.198. The flow patterns for $\alpha = 5$ deg are shown in Fig. 16b. The flow continues to look smooth and attached on the forward parts of the wing. There appears to be a region of vortex flow near the base of the root chord and slight areas of separation are evident along the tip regions of the trailing edge. Some slight areas of separation near the leading edge are verified by the accompanying vapor-screen photographs. A weaker vortex is partially hidden by the wing camber.

At 0 deg angle of attack, the flat wing displays the smoothest flow pattern, but this pattern apparently degenerates rapidly with angle of attack as does performance. These photographs clearly show that the severely constrained wing displays the desired characteristic of being able to suppress the formation of vortices and separation to a higher angle of attack, thus explaining why it achieved the best performance at the higher lift coefficients.

Concluding Remarks

Comparisons of experimental data with three different theoretical prediction methods for a set of twisted and cambered supersonic wing models indicated that drag levels were generally underpredicted by linear theory methods and overpredicted by the nonlinear methods, especially at the lower lift coefficients. Unlike the cambered wing results, experimental drag levels on the flat wing are lower than predicted by either the linear or nonlinear methods, indicating that more thrust or vortex lift benefits were achieved than were predicted. On all wings, the pitching moment data were best predicted by the nonlinear theory with available and vortex lift.

The flow-visualization photographs of all wing models show vortices developing near the nose region of the leading edge. It may be that the large change required in flow direction from the nearly blunt nose to the highly swept inboard region is causing the formation of the nose vortex. Elimination of the blunt apex region of the nose should reduce this problem.

Vortex strength and separation regions are mildest at $\alpha = 5$ deg for the wing designed to have $\Delta C_D = 0$ at the leading edge

at the design C_L of 0.08. Thus, the results of this investigation indicate that while the severe constraint on leading-edge pressures does cause a penalty in the performance of that wing at the lower lift coefficients, it also delays the formation of vortex flow and separation, resulting in better performance than the other wings at the higher C_L values. Based on the improved performance at high lift, future designs which require high-lift flight and maneuver performance may indeed benefit from the approach used in designing these wings.

References

[1]Robins, A. W., Lamb, M., and Miller, D. S., "Aerodynamic Characteristics at Mach Number of 1.5, 1.8, and 2.0 of a Blended Wing-Body Configuration With and Without Integral Canards," NASA TP 1427, 1979.

[2]Kulfan, R. M. and Sigalla, A., "Real Flow Limitations in Supersonic Airplane Design," AIAA Paper 78-147, 1978.

[3]Carlson, H. W. and Miller, D. S., "Influence of Leading-Edge Thrust on Twisted and Cambered Wing Design for Supersonic Cruise," *Journal of Aircraft*, Vol. 20, May 1983, pp.

[4]Middleton, W. D. and Lundry, J. L., "A System for Aerodynamic Design and Analysis of Supersonic Aircraft: Part 1—General Development and Theoretical Development," NASA CR 3351, Dec. 1980.

[5]Middleton, W. D., Lundry, J. L., and Coleman, R. G., "A System for Aerodynamic Design and Analysis of Supersonic Aircraft: Part 2—User's Manual," NASA CR 3352, Dec. 1980.

[6]Middleton, W. D., Lundry, J. L., and Coleman, R. G., "A System for Aerodynamic Design and Analysis of Supersonic Aircraft: Part 3—Computer Program Description," NASA CR 3353, Dec. 1980.

[7]Carlson, H. W. and Mack, R. J., "Estimation of Wing Nonlinear Aerodynamic Characteristics at Supersonic Speeds," NASA TP 1718, Nov. 1980.

[8]Miller, D. S. and Wood, R. M., "An Investigation of Wing Leading Edge Vortices at Supersonic Speeds," AIAA Paper 83-1863, 1983.